Thermal Spray 2003: Advancing the Science & Applying the Technology, (Ed.) C. Moreau and B. Marple, Published by ASM International, Materials Park, Ohio, USA, 2003

Influences of Substrate Roughness and Temperature on Adhesive Strength in Thermal Spray Coatings

H. Fukanuma, N. Ohno
Plasma Giken Co., Ltd., Toda City, Saitama, Japan

Abstract

It is essential to understand and clarify what causes adhesive strength between the thermally sprayed deposit and the substrate. It is known that the adhesive bond strength is strongly related to the roughness of the substrate surface [1-3], however, we are yet to know why and how the roughness affects the strength. Although the roughness works as a so-called anchor or interlocking effect, we cannot show how the effect quantitatively relates to the strength. Before we use the word "roughness", we need to define roughness as a strict meaning in connection with the adhesive strength to avoid any ambiguity in expressing the roughness itself. Seeking the true roughness to relate to the bond strength, we have introduced a newly developed roughness indicator correlated closely with the adhesive strength. This indicator is derived by theory on the basis of the assumption that the bond strength is primarily caused by the mechanical friction between the deposit and the substrate [4]. It was supposed that chemical and physical adhesions were secondary effects except that the molten particle, the substrate temperature or both of them are high enough to form these bonds by thermal interaction.

The increase in contact area between the splat and the substrate could raise the friction force between them. The higher substrate temperature could increase the contact area when the molten particle interacts with the substrate, because the molten particle could wet better on the high temperature substrate. The substrate temperature influence on the adhesive strength was also investigated.

Introduction

The adhesion of thermal spray coatings has been explained by three primary mechanisms, mechanical anchorage and physical or chemical interaction. These mechanisms are still not fully understood and have only been explained qualitatively in strength, not quantitatively. The anchor effect is the predominant mechanism, except for deposits sprayed in high contact temperature conditions.

It is well known that the substrate surface roughness strongly affects the bond strength. Although studies on morphology of roughened surfaces have been reported [5 – 8], investigations that seek numerical relations between the roughness and the adhesion are still few. Some researchers have attempted numerical studies on influences of the roughness on the adhesion. Siegmann et al reported the fractal or area scale fractal complexity had good correlation with the adhesive strength [9, 11]. Amada et al also studied the relations between fractal dimensions of the roughness and the strength [12, 13]. However, their investigations were still lacking clear physical interpretations how the roughness affects the strength. We reported a model that characterizes the roughness in a new way that described the quantitative relation between the adhesion and the roughness in the previous paper [4].

The basic idea of the model

We assume that the adhesive strength is caused by mechanical friction force between the deposit and the roughened substrate. Suppose that a thin object is placed on an inclined plane as shown in Fig. 1. If pressure P is applied to the interface between the object and the slope, the friction force f is characterized as;

$$f = \mu P s \qquad 1$$

where "μ" and "s" are friction coefficient and the contact area between the object and the slope, respectively. We need force f_v to vertically remove the object from the slope against the friction force. The separation force f_v is expressed as;

$$f_v = f\cos\theta = \mu P s\cos\theta \qquad 2$$

Equation 2 shows that the removal force f_v is proportional to the projection area "$s\cos\theta$" that is obtained by projecting "s" onto a perpendicular plane.

Let's think about an ideal surface roughness that is formed by pyramids as shown in Fig. 2. In the pyramid dimensions, the height is "h" and a side length of the base is "a". Suppose

that the ideal roughened surface is covered with a thermally sprayed deposit, the force to remove the deposit from a slope plane in a pyramid is shown in Eq. 2. Since the slope area "s" and $\cos\theta$ are expressed as the following equations, respectively, in the case of the pyramid.

$$s = \frac{1}{2}a\sqrt{h^2 + \frac{a^2}{4}} \qquad 3$$

$$\cos\theta = \frac{h}{\sqrt{h^2 + \frac{a^2}{4}}} \qquad 4$$

Substituting Eq. 3 and Eq. 4 into Eq. 2, we can obtain the removal force f_v as the following equation.

$$f_v = \mu P s\cos\theta = \frac{1}{2}\mu P a h \qquad 5$$

Since one pyramid has four slope planes, the separation force to remove the deposit from one pyramid is $4f_v$. The total force to remove the deposit form the ideal rough surface shown in Fig. 2 is $35\times 4f_v$ because the surface has 35 pyramids. Since the substrate area is $l_1 \times l_2$, the removal force on a unit area "F" is expressed as the following equation.

$$F = \frac{35\times 4f_v}{l_1 \times l_2} = \mu P\left(\frac{2h}{a}\right) \qquad 6$$

Since "F" means the adhesion strength, we define the term "$2h/a$" in Eq. 6 as the roughness "R_{bz}". Then Eq. 6 is reduced to the following equation.

$$F = \mu P R_{bz} \qquad 7$$

We have thus obtained the roughness based on the new idea that the adhesion relates to mechanical friction force.

If the height or the side length of the pyramid changes, the roughness will change. The number of the pyramids on the substrate surface also changes the roughness. We can also obtain the roughness in which case even various types of pyramids are placed on the substrate. We can easily generalize the model and apply it to conventional roughness such as a grit blasted surface.

Generalization of the model

We can apply the basic idea to an actual rough surface. Suppose that a thermally sprayed deposit covers a rough surface that is expressed as the following function in orthogonal coordinates (O, x, y, z).

$$z = f(x, y) \qquad 8$$

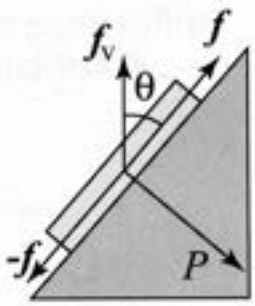

Fig.1: Schematic illustration of mechanical friction force applying to the interface between a thin object and a slope plane.

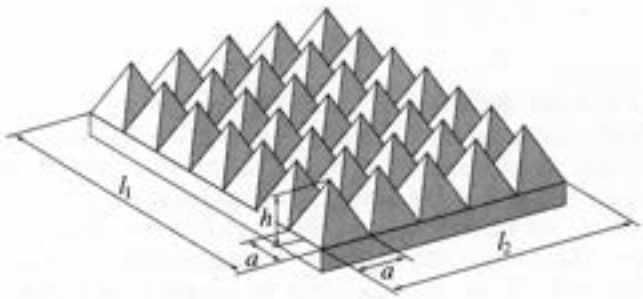

Fig. 2: An ideal roughness formed by pyramids.

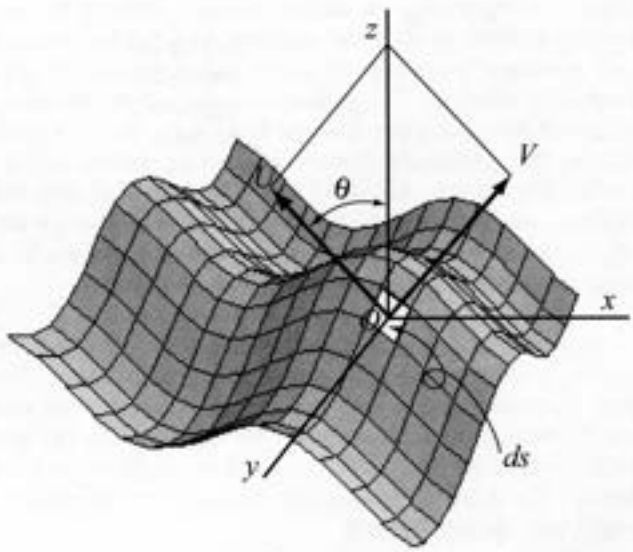

Fig. 3: Schematic illustration of friction force applied to an infinitesimal element on a rough surface.

Then, the force "df_v" to vertically remove the deposit on the infinitesimal area "ds" of the surface is expressed as the following equation,

$$df_v = \mu P ds\cos\theta \qquad 9$$

where "θ" is the angle zOU as shown in Fig. 3.

Line OV is the normal line of ds, line OU is on the plane formed by line OV and Oz and tangent to the surface element "ds" at the point "O". The least force to separate perpendicularly the deposit from the rough substrate domain "D" is expressed as the following equation,

$$\int_D df_v = \int_S \mu P \cos\theta ds \qquad 10$$

where "S" is all the roughened surface area within the domain "D". Since both friction coefficient "μ" and pressure "P" are actually functions of "x" and "y", the integration of Eq. 10 is impossible until the real function forms of "μ" and "P" are obtained. If we can replace "μ" and "P" with average friction coefficient $\overline{\mu}$ and pressure $\overline{P}$ on the surface area "S" in the domain "D", the next equation holds.

$$\int_D df_v = \int_S \mu P \cos\theta ds = \overline{\mu}\overline{P}\int_S \cos\theta ds \qquad 11$$

The adhesive strength per unit area "F" is expressed as the following equation.

$$F = \frac{\int_D df_v}{D} = \frac{\overline{\mu}\overline{P}\int_S \cos\theta ds}{D} \qquad 12$$

If we can obtain three dimensional data of the surface profiles of the rough surface, the integration term in equation 12 can be calculated, and, we have thus obtained a method to predict theoretically the adhesive strength of the thermal sprayed deposit on the roughened substrate. We introduce the roughness indicator "R_{bs}" defined as follows,

$$R_{bs} = \frac{\int_S \cos\theta ds}{D} \qquad 13$$

then, substituting Eq. 13 into Eq. 12, Eq. 12, the next expression is obtained.

$$F = \overline{\mu}\overline{P}R_{bs} \qquad 14$$

We give the name "bond strength roughness" to "R_{bs}".

Roughness measurement

If we can obtain "R_{bs}" of the substrate, we can evaluate the roughness in connection with the adhesive strength. To obtain "R_{bs}", we have to measure the surface profile with three dimensional measurement methods and use computer processing for the results. There are several measuring techniques of surface roughness, contact or noncontact method [8]. Confocal scanning microscopy has advantages in measuring such degrees of roughness for the substrate preparation by grit blasting before thermal spray [14]. The measuring method is a noncontact process with high resolution and high measuring speed. To compute "R_{bs}" from 3-D measurements with the confocal microscopy, new program code was developed [4].

Experiment procedures and results

Grit blasting: Aluminum and stainless steel specimens were used for grit blasting and tensile bond test of plasma spray deposits. The specimen dimensions are 20 mm in diameter and 40 mm in length. Conventional suction type blasting equipment was used with the newly developed grit feeder to secure feeding rate accuracy and reproducebility. A six-axis robot was mounted on the equipment to control the traverse speed, pitch, stand-off distance and nozzle angle. The grit material was #100 alumina, and the nozzle internal diameter was 9 mm. The grit blasting conditions are shown in Table 1 and the specimen conditions are also shown in Table 2.

Table 1: Blasting conditions

Traverse speed	1000 mm/sec
Traverse pitch	10 mm
Stand-off distance	120 mm
Nozzle angle	Rectangular
Feed rate	700 g/min.
Blasting air pressure	0.5 Mpa

Table 2: Specimen conditions

Test number	Number of blasting passes	Specimen material	Number of specimens
#1	2	Aluminum	20
#2	5	Aluminum	20
#3	10	Aluminum	20
#4	20	Aluminum	20
#5	2	Stainless steel	20
#6	5	Stainless steel	20
#7	10	Stainless steel	20
#8	20	Stainless steel	20

One of twenty test pieces in each condition was measured for 3-D morphology with the Lasertec confocal microscope, HD100D (Lasertec Inc. Yokohama, Japan). Five places on each specimen were measured. Then, data processing was carried out and the average of five measured results was adopted as bond strength roughness "R_{bs}". The measurement area was about 350x350 μ m and the resolution was 0.42 μ m. The resolution of the height was 0.01 μ m. Confocal microscopic images of test piece #1 and #4 are shown in Fig. 4 and 5. We can see that #4 apparently has much more complexity in surface morphology than #1. Specimen #4 was blasted in 20 passes while #1 was 2 passes.

The bond strength roughness "R_{bs}" versus the number of blasting passes is shown in Fig 6. The graph shows that "R_{bs}" increases as the number of blasting passes increases. The aluminum test pieces were roughened faster than the stainless steel.

Plasma spraying: After the specimens were grit blasted, about 500 μ m of white alumina was deposited on them. The specimens were preheated to investigate the influence of the substrate temperature. The test pieces in every group of blasting passes were preheated to room temperature, 100 C, 200 C, or 300 C. The deposited test pieces were measured for adhesive strength in accordance with Japanese industrial standard H8664.

Table 3: Plasma spray conditions

Plasma torch	Praxair SG-100
Arc current	850 A
Arc voltage	38 V
Arc gas Ar	50 PSI
Secondary gas He	100PSI
Traverse speed	1000 mm/sec
Traverse pitch	4 mm
Stand off distance	100 mm
Powder feed rate	20 g/min
Spray material	White alumina 10-44 μ m

Table 4: Conditions of internal fracture of the deposits

Test piece material	Number of blasting passes	Preheating temperature	Fracture interface
Aluminum	20	200°C	Deposit inside
	2	300°C	
	5		
	10		
	20		
Stainless steel	20	300°C	

The experimental results of adhesive strength (the averages of every five specimens) versus the roughness indicator "R_{bs}" with substrate temperatures are shown in figure 7 and 8. All the fracture interfaces on aluminum sprayed at 300 °C were within the deposits (cohesive failure), and the deposits on the substrate with 20 passes of blasting and at 200°C of preheating temperature were also broken in the insides of the coatings. The deposits on the stainless steel specimens with 20 passes of grit blasting and at 300 °C of preheating temperature were also broken within the coatings. The other fracture interfaces were between the substrate and the deposit. The conditions in which internal fracture occurred are shown in Table 4, when the tensile bond strength tests were carried out. Figure 7 and 8 show that the adhesive strength on both aluminum and stainless steel substrates increases as "R_{bs}" increases except the cases in which internal fracturing took place.

Figure 9 shows that the adhesive strength on aluminum substrate is greatly influenced by the preheating temperature. The higher substrate temperature produces higher bond strength of aluminum oxide on aluminum substrate, while the bond strength on stainless steel appears to be insensitive to the substrate temperature as shown in Fig. 10. To obtain higher bond strength on stainless steel, temperatures higher than 300°C could be necessary. The strength on the aluminum substrate at room temperature is lower than that on the stainless steel substrate. The maximum adhesive strength on aluminum is nearly the same as that on stainless steel.

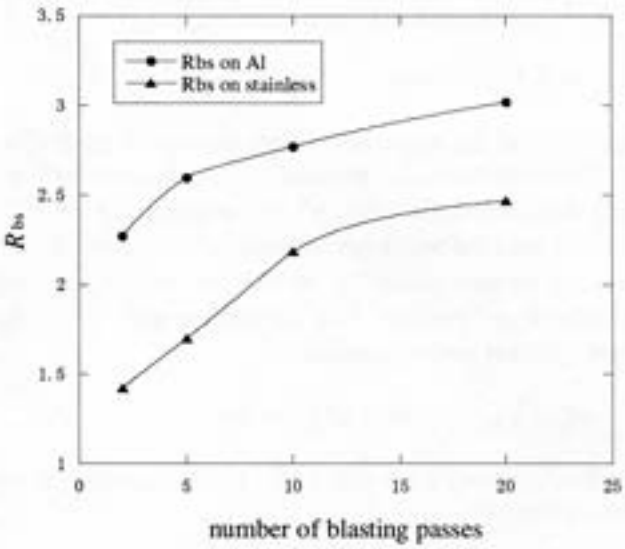

Fig. 6: The relationship between the bond strength roughness "R_{bs}" and the number of blasting passes on aluminum and stainless steel substrates.

Discussion

The experimental results seem to show the bonding strength roughness "R_{bs}" has strong correlation with adhesive strength, thus it appears to be correct that adhesive strength mainly derives form mechanical friction force. Linearity is lacking in the relations between the adhesive strength and the roughness "R_{bs}" in graph 7 and 8. This could be because of physical or chemical effects or both, or because of the influence of voids that cannot be measured with confocal microscopy. The characterization method of the morphology on the roughened surface in this model appears to be able to clarify the understanding of the bonding mechanism of thermal spray coatings. To further explain whether the assumption is correct or not, more precise bond strength experiments are necessary with various spray materials on many kinds of substrate materials. We used only aluminum oxide in these experiments and avoided metal materials at this time because of our intention to minimize chemical and physical mechanisms.

As shown in Fig. 6, the roughness "R_{bs}" on the aluminum substrates is larger than that on the stainless steel, but the bond strength on the aluminum is lower than that on the stainless steel sprayed at room temperature and 100°C. The contact area between the alumina splats and the aluminum substrate could be smaller than that between the splat and the stainless steel causing the friction coefficient on aluminum to be smaller than that on stainless steel. The reason might be that the aluminum substrate has less wettability because of the high heat conductivity of aluminum.

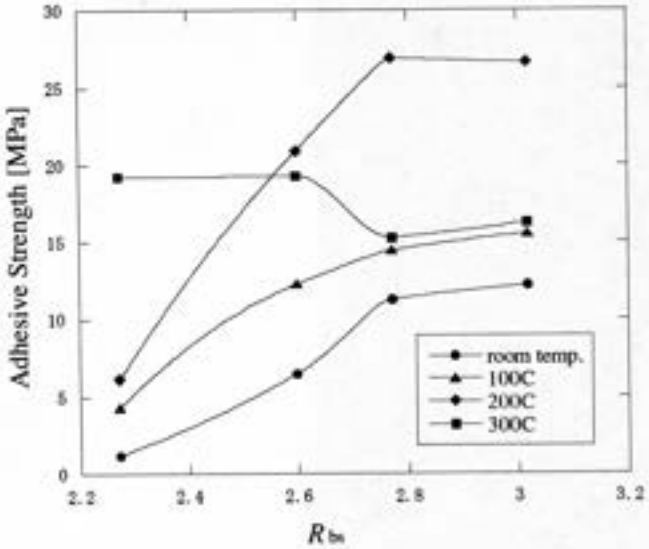

Fig. 7: The relationship between adhesive strength and the bond strength roughness "R_{bs}" on the aluminum substrates with the preheating temperature.

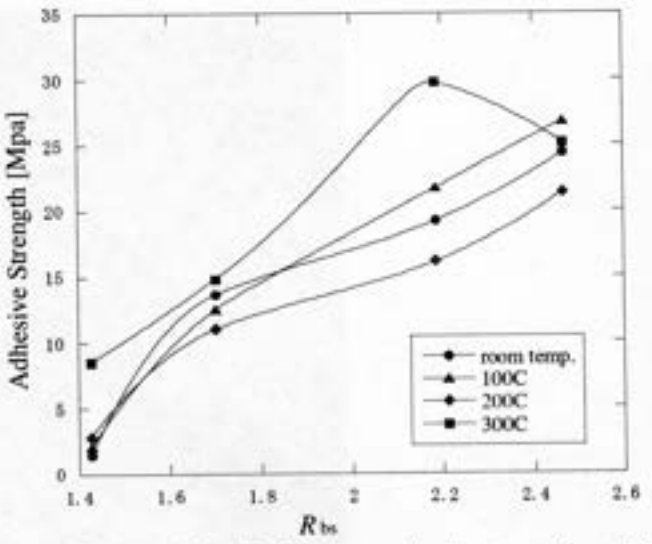

Fig. 8: The relationship between adhesive strength and the bond strength roughness "R_{bs}" on the stainless steel substrates with the preheating temperature.

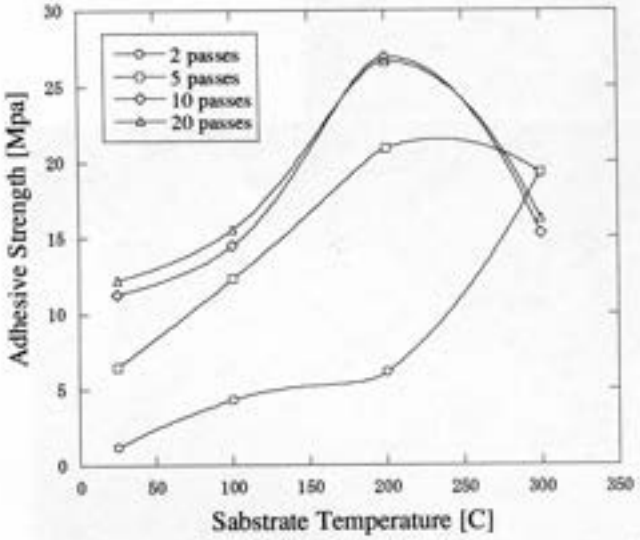

Fig. 9: The relationship between the adhesive strength and the aluminum substrate with the number of blasting passes

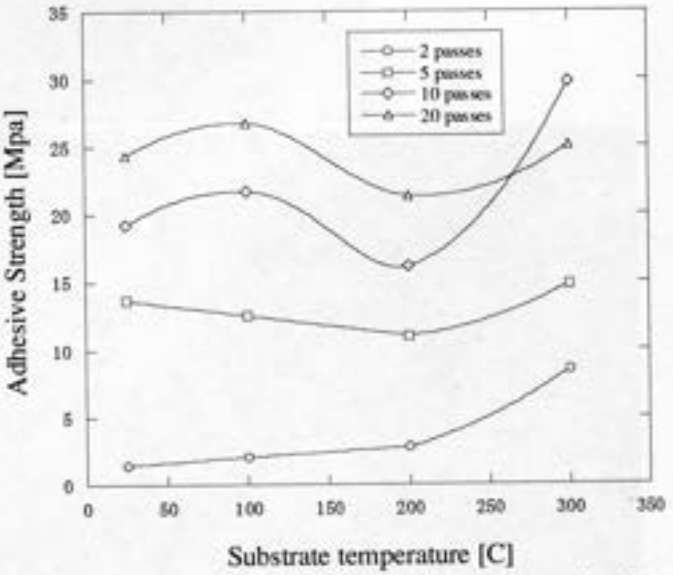

Fig. 10: The relationship between the adhesive strength and the stainless steel substrate with number of blasting passes

The adhesive strength on the aluminum substrate is much more temperature sensitive than that on the stainless steel as shown in Fig. 9 and 10. The reason could be that the wettability of alumina splats on aluminum strongly depends on the substrate temperature, because the aluminum substrate quickly absorbs heat inside the splats due to its high thermal conductivity so that the splat temperature could rapidly drop, then, the splats do no easily wet the substrate. On the other hand, since the thermal conductivity of stainless steel is much lower than that of aluminum, the splats on stainless steel wet the substrate well with small dependence on the substrate temperature.

Conclusions

The roughness indicator "R_{bs}" shows good correlation with the adhesive bond strength of the alumina deposits on the aluminum and stainless substrates. This model appears to be effective for evaluating substrate roughness in relation to bond strength.

The bond strength of the alumina on the aluminum substrate is greatly influenced by the substrate temperature.

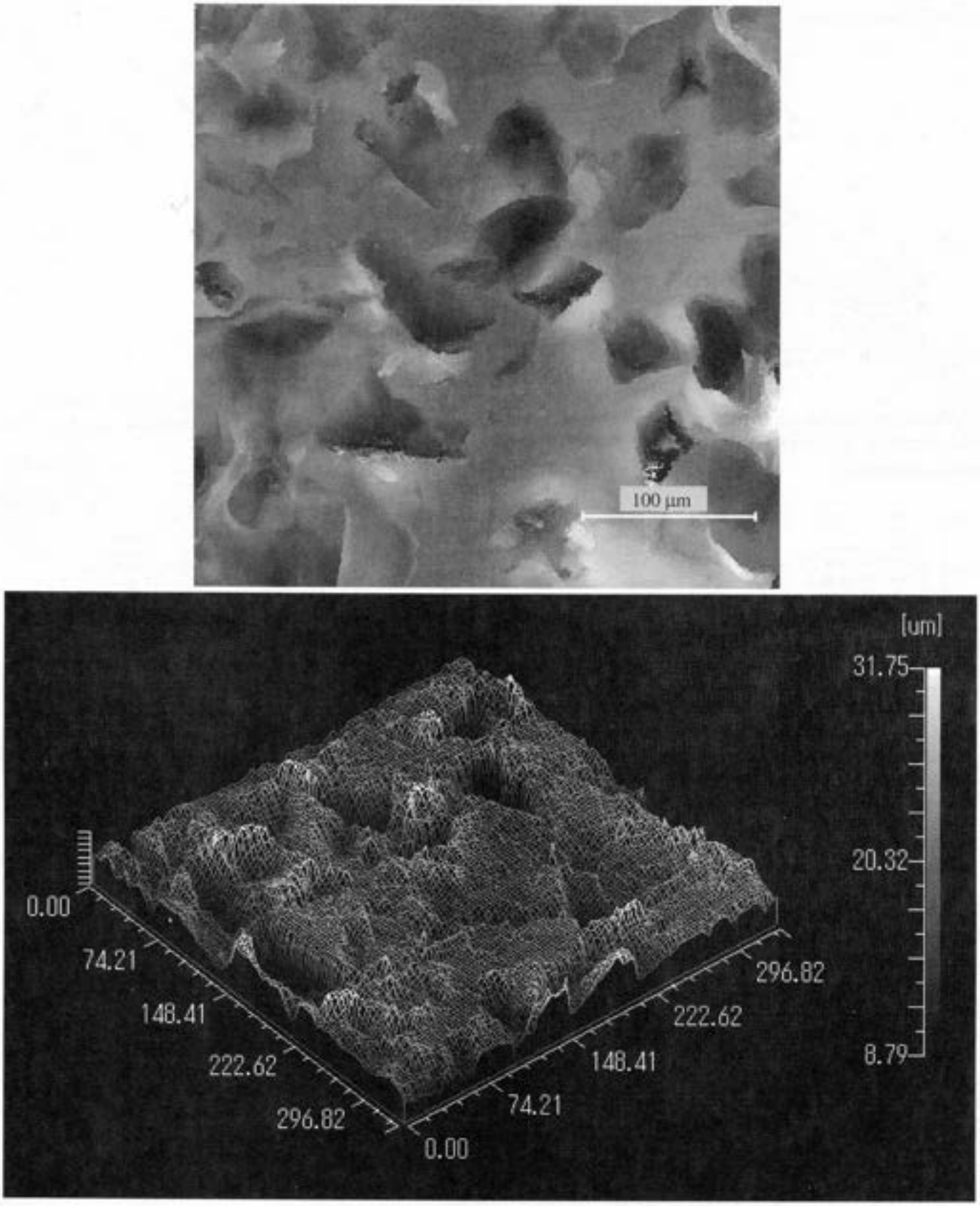

Fig.4: Image of roughened aluminum surface after two blast passes.

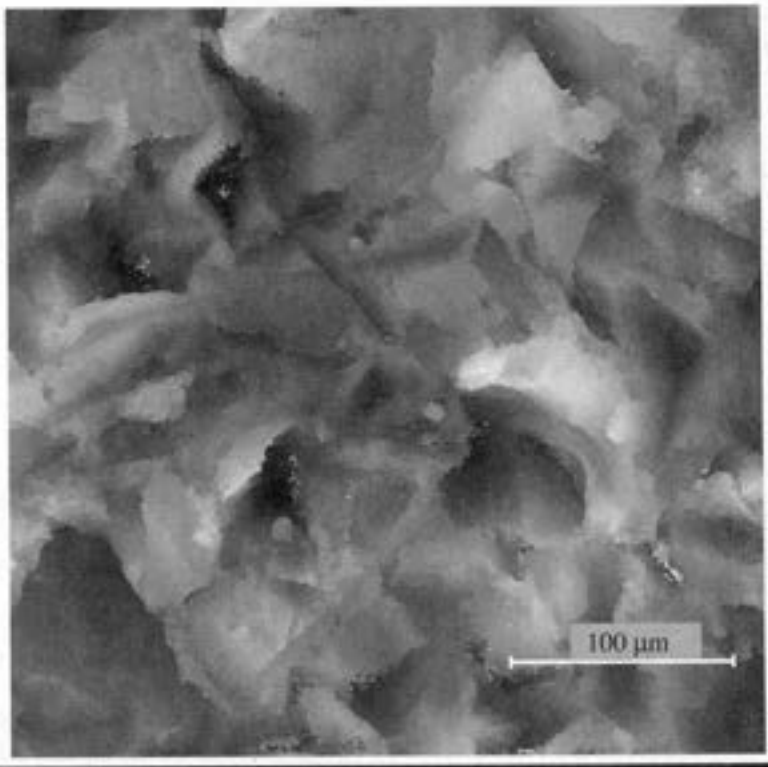

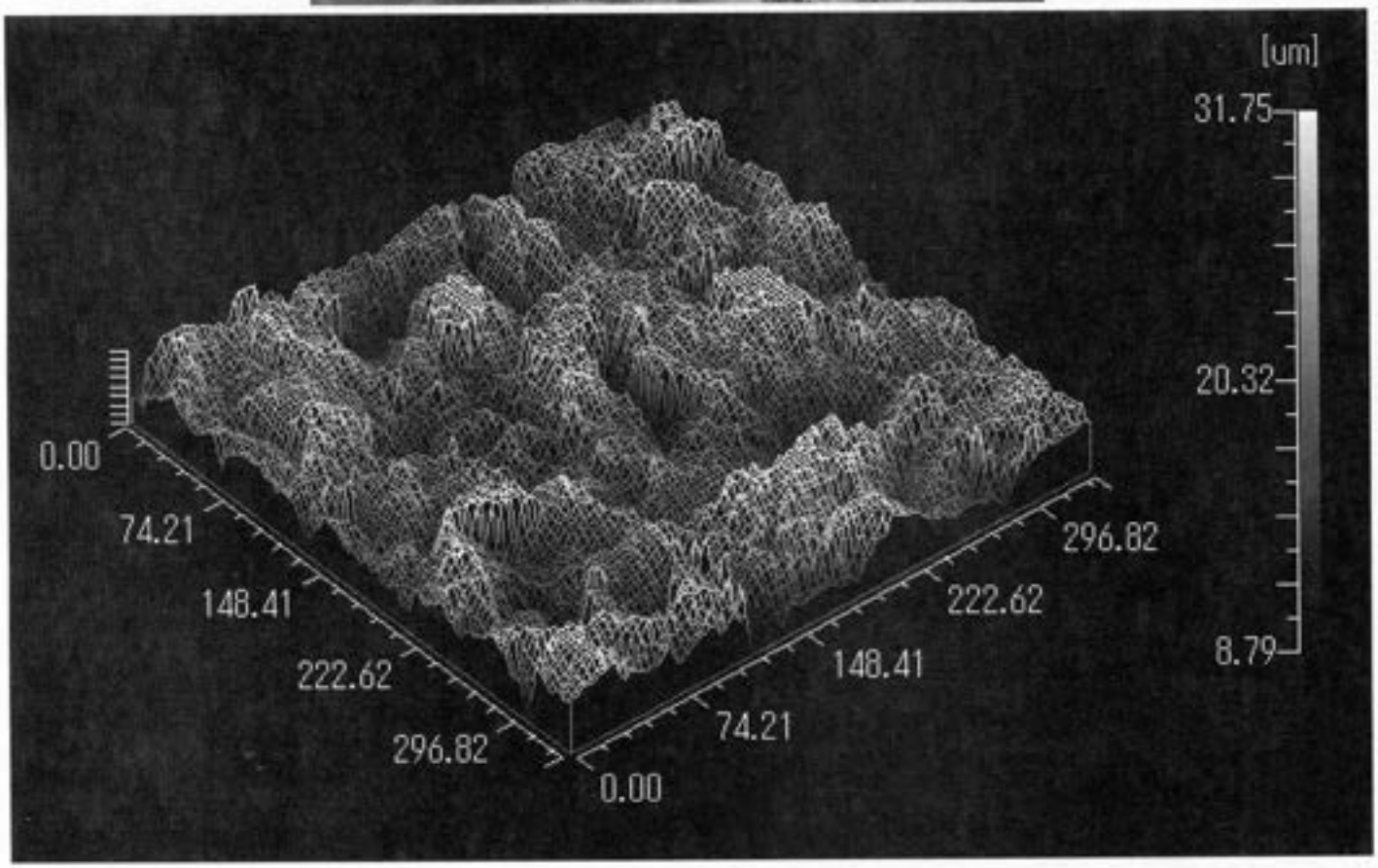

Fig. 5: Image of roughened aluminum surface after twenty blast passes.

Confocal scanning microscopy is useful to measure the 3-D profile on roughened substrate surface because of its high resolution, surface noncontact method and high measurement speed.

References

1. D. Matejka and B. Benko, *Plasma Spraying of Metallic and Ceramic Materials*, John Wiley and Sons Ltd., West Sussex, England, 1989, pp. 91-95.
2. R. B. Heimann, *Plasma-Spray Coating*, VCH, Weinheim, Germany, 1996, pp. 167-168
3. L. Pawlowski, *The Science and Engineering of Thermal Spray Coatings*, John Wiley & Sons, West Sussex, England, 1995, pp.127-130.
4. H. Fukanuma., R. Xie., N. Ohno, Y. Fujiwara and S. Kuroda, Characterization of Roughened Substrate Surface on Bond Strength of Thermal Spray Deposits, ITSC 2002 3Conference Proceedings, pp.312/317
5. J. Wigren, Grit-Blasting As Surface Preparation Before Plasma Spraying. Advances in Coatings Technology, 1987 NTSC, pp. 99/104.
6. M. Mellali, A. Grimaud and P. Fauchais, Parameters Controlling the Blasting of Substrates for Plasma Spray, Thermal Spray Industrial Applications, 1994, pp. 227/232.
7. S. J. Yankee, B. J. Pletka and R. L. Salsbury, Quality Control of Hydroxylapatite Coatings, The Surface Preparation Stage: Properties, Processes and Applications, 1991, pp.475/479
8. K. Pathasarathi, K. Sampath and B. R. Tittmann, Metrology of Grit Blasted Surface, Advances in Thermal Spray Science and Technology, 1995, pp. 505/513.
9. S. D. Siegmann and C. A. Brown, Scale-Sensitive Fractal Analysis for Understanding the Influence of Substrate Roughness in Thermal Spraying, Thermal Spray: A United Forum for Scientific and Technological Advances, 1997, pp. 665/670.
10. S. D. Siegmann and C. A. Brown, Investigation of Substrate Roughness in Thermal Spraying by A Scale-Sensitive 3-D Fractal Analysis Method, Thermal Spray: Meeting the Challenges of the 21st Century, 1998, pp. 931/836.
11. S. D. Siegmann and C. A. Brown, Surface texture correlations with tensile adhesive strength of thermal sprayed coatings using area-scale fractal analysis, 1999 United Thermal Spray Conference Proceedings, pp. 355/360.
12. S. Amada, H. Yamada, S. Yematsu and Y. Saotome, Modeling and Measurement of Adhesive Strength of Thermal Sprayed Coatings, International Advances in Coatings Technology, 1992, 915/920.
13. S. Amada, T. Hirose and K. Tomoyasu, Introduction of Fractal Dimension to Evaluation of Adhesive Strength, Current Status and Future Trends, 1995, pp. 885/890.
14. Confocal Microscopy edited by T. Wilson, 1990 Published by Academic Press Limited, pp. 7/30.